



Design and Implementation of the Rotor Blades of Small Horizontal Axis Wind Turbine

Tamer Nabil*, Mohamed Khairat Dawood, Tamer Mansour

Mechanical Engineering Department, Suez Canal University, 51422, Egypt.

PAPER INFO

Paper history:

Received 21 February 2019

Accepted in revised form 31 March 2019

Keywords:

Small horizontal wind turbines
Airfoil
XFOIL
QBlade
MATLAB
CFD

ABSTRACT

Since the renewable resources of energy have become extremely important, especially wind energy, scientists have begun to modify the design of the wind turbine components, mainly rotor blades. Aerodynamic design considered a major research field related to power production of a small horizontal wind turbine, especially in low wind speed locations. This study displays an approach to the selection of airfoil and blade design utilized in small horizontal wind turbines with low cut-in speed and with no gear box. Modeling of the flow depends on Computational Fluid Dynamics (CFD) and theory of Blade Element Momentum (BEM) methodologies. QBlade used (BEM) for wind turbine simulation and integrated with XFOIL for airfoils design to ensure the requested characteristics for wind turbine performance. MATLAB is used to calculate the final design parameters to be modeled in SOLIDWORK. The flow dynamics are explored with the aid of ANSYS Fluent 16. The application of specially designed blades grants start up at lower wind speeds. The designed blade is fabricated from polyurethane foam. Experimental study confirmed that, at low average wind velocity (4 m/s), the fabricated small-scale horizontal wind turbines are considered to be a positive way to supply electricity with an average power rate of 9 watt and efficiency of 8 %.

1. INTRODUCTION

Energy sources are grouped into non-renewable and renewable, which includes wind energy. The expense of wind power is much lower than that of other renewable sources. Accordingly, as the most encouraging power source, wind power is accepted to assume a basic job in power supply and must be investigated [1]. Wind turbine goes through several developments and modifications. Therefore, wind turbines could operate at low wind speeds on a small scale and are adjusted for special applications.

Nowadays, small-scale horizontal axis wind turbines are receiving great attention and promising output, especially in the developing countries and remote areas, where the electrical framework is inaccessible. In this regard, the classic three-bladed horizontal axis wind turbine is the preferred choice [2].

Egypt has shown a great ambition about the development of renewable energy resources since 1986. Records in 2016 show that 3 % of electricity has been generated out of renewable resources such as wind and solar. The Egyptian New & Renewable Energy policy aims to raise the portion of electricity generated from wind to 2.5 % by 2022. The high-share percentage of wind power will be satisfied by large and small wind turbines [3]-[5]. It has been found that advances in blade aerodynamics design may contribute to an increase in the energy income of wind turbines. Records on wind directions and speeds for the planned site location of turbine establishment are significant issues for a precise investigation of a wind turbine performance. The site location of this study is selected in Ismailia (30.35° N, 32.16° E), Egypt with an average wind speed of 4 m/s.

2. LITERATURE REVIEW

Many scientists have investigated the horizontal axis wind turbines to prove that the performance of upwind turbines is higher than the downwind ones [6]. Airfoil and blade aerodynamic design is considered as the key to the wind turbine performance. Several codes appeared to enhance these designs such as XFOIL, PROFOIL, and Eppler [7]. The blade with a high power coefficient and a ratio of lift to drag is favored. In the simulation process, $k-\omega$ SST (shear stress transport) is considered as a promising turbulence model. Costa Rocha et al. [8] used the $k-\omega$ SST turbulence model for a small wind turbine to compare symmetric and cambered airfoils. They designed two sets of blades for a small-scale wind turbine. The first with an NACA 0012 airfoil (symmetrical) and the other with an NACA 4412 airfoil (cambered). As expected, the turbine designed with the NACA 4412 airfoil yielded the highest C_p values. This fact brings the NACA 4412 blades closer to the assumptions of the BEM model, which usually discards the drag effects. It was found that β^* values suggested above by the $k-\omega$ SST turbulence model were more appropriate. The $k-\omega$ SST turbulence model showed itself to be suitable for the numerical simulation of small-scale wind turbines.

There are several techniques to design the blades and evaluate the performance; however, the Blade Element Momentum theory is the favorable one. Bai et al. [9] showed that the BEM theory was very successful in HAWT blade design. The modification factor and models were also combined into the BEM theory to predict the blade performance, and there is a good comparison of torque and thrust in each section between the improved BEM theory and numerical simulation. The detailed flow fields were also investigated based on the fully 3D CFD simulations by means of the commercial code Fluent and the $k-\omega$ SST turbulence

*Corresponding Author's Email: tamer_mtc@yahoo.com (T. Nabil)

model, and also showed that the Fluent package could be used to calculate the performance of an HAWT blade.

Several parameters must be calculated to evaluate the blade performance such as power coefficient, lift-to-drag ratio, number of blades, angle of attack, tip speed ratio, and wind speed. Chaudhary and Roy [10] found that the maximum power coefficient was obtained for solidity in the range of 3 % to 12 % for blades 3, 5, and 7. The Rotor performance is optimum if the pitch angle is in between 0° to 3° . If the blade number is increased from 3 to 7, then power coefficient values increase up to 10 %. If blade number changes from 3 to 5, then the annual energy production is increased to 8 %; however, if it changes from 5 to 7, then the annual energy production is reduced by 4 %. Electrically rated power produced by 5-bladed wind turbines is 10 % and 8 % more than those by 3-bladed and 7-bladed wind turbines, respectively, corresponding to a rated wind speed of 8 m/s.

The Computational Fluid Dynamics (CFD) technique produces promising results regarding the blade performance [11]. Juliayana et al. [12] used ANSYS CFD software, and showed that the blade with a constant angle of attack was analyzed throughout the length to find a blade with a maximum L/D ratio. This was done for the angle of attack ranging from 3° to 10° , and it was found that a blade with 4° angle of attack had the maximum L/D ratio, leading to an increase in the efficiency. The two-dimensional model of NACA4420 aero-foil was created in Solid Works, and the blades were analyzed in 4 sections.

Meng-Hsien Lee et al. [13] has researched in experiments and numerical simulations of the rotor-blade performance for a small-scale HAWT to investigate the aerodynamic performances of the BEMT-blade rotor and the Baseline-blade rotor used in a HAWT system. They found that the flow fully attaches to the entire BEMT-blade without separation, while the flow attachment covers only a partial region above the 76 % span of the Baseline blade. Thus, a difference between the resulting torque values and their optimal power coefficients can be observed. Prasad and Vardhan [14] noticed that all the blades were capable to bear the maximum loading value when applied at the root section and the blades would fail at a lower magnitude of loading.

BEM theory does not consider the turbulence effects. Therefore, the values of power coefficient in QBlade analysis results are higher than those of CFD analysis results.

Koc et al. [15] concluded that the blade of a 2 m wind turbine had NACA4412 airfoil, which was modeled on Fluent with SST k- ω and Qblade. Maximum torque was obtained as 31 N.m in Qblade and 28 N.m in Fluent. The maximum power coefficient value was obtained as 0.48 in Qblade and 0.45 in Fluent.

Ali et al. [16] investigated the winglet effect on the aerodynamic performance of the wind turbine blade used for a domestic-scale wind generator. The results indicated an increase in the lift-to-drag ratio with the upwind winglet by around 26 % compared to a straight blade with no winglet, whereas the downwind winglet resulted in a decrease in the lift-to-drag ratio about 27 %. Additionally, the yaw angle of the turbine blade plays an important role in ensuring better aerodynamic performance. The results indicate that the maximum aerodynamic performance can be achieved between 0° and -30° yaw angle.

There are several researchers who have investigated, modified, and optimized the aerodynamic performance of small wind turbines based on the blade design taking into

consideration several aspects such as low wind speed, numerical assumptions and calculations, simulation techniques, and manufacturing processes [17-22].

Considering the results of the aforementioned previous studies and the suffering of the world in general and Egypt in particular, or remote areas, energy should be used from any related resources, even if the extracted amount of energy is weak. This paper designed and fabricated small horizontal axis wind turbine blades in low wind speed locations despite the expectation of low-scale energy extracted from them.

3. AIRFOIL DESIGN AND SELECTION

The lift and drag forces arise from the motion of an airfoil-shaped body in a fluid and characterize the blade performance [2]. Optimal lift can be obtained by angle of attack and airfoil shape adaptation. Various standard airfoils are available through which the small horizontal axis wind turbine blade profiles can be developed. Aerodynamic concepts associated with the selected airfoils need to be investigated.

Aerodynamic behavior, low weight, and structural reliability of the blade affect the process of selecting proper airfoils. The best airfoil is carefully selected from an initial group of eight airfoils, which were carefully chosen according to surveys, site wind conditions, required power, and applications. Since the scheduled wind turbine site was at its low Reynolds number location, the simulation analysis was performed by XFOIL software. The considered eight airfoils include [23] Bergy BW-3 (smoothed), E387, NACA 64 (3)-418, NREL's S809, S7012 (8.75 %), SD2030-086-88, SD7062 (14 %), and SG6043. Based on numerical calculations, the obtained maximum Mach number is 0.2 due to low wind speeds. The critical amplification ratio " N_{crit} " of the free transition criterion value was 9. The angle of attack ranged between -5 and 25 degrees.

Inviscid flow can be simulated in XFOIL by using the integration of steady Euler equations [24]. Airfoils were simulated on XFOIL at different Reynolds numbers 4×10^5 , 4.5×10^5 , and 5×10^5 ; from the obtained data, the values of the lift, drag, and lift to drag coefficients were calculated at different angles of attack, as shown in Figures 1, 2, and 3.

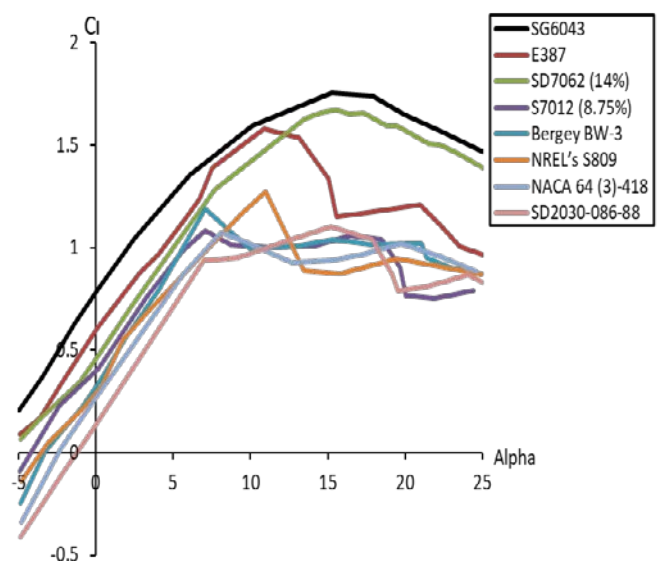


Figure 1. Lift coefficient-angle of attack relations for different airfoils at $Re=5 \times 10^5$.

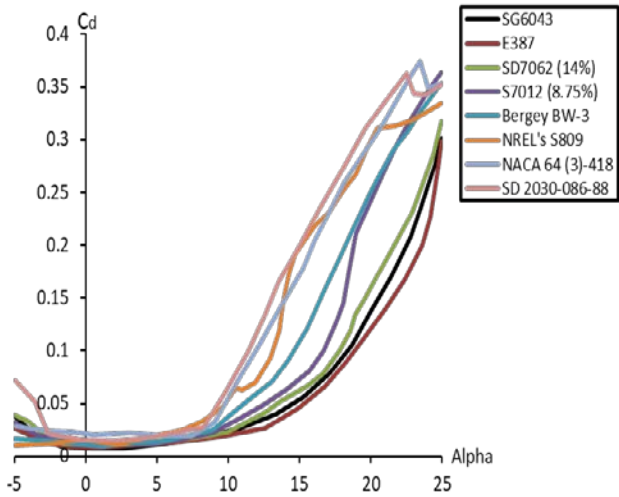


Figure 2. Drag coefficient-angle of attack relations for different airfoils at $Re=5*10^5$.

Figures 1, 2, 3 show that SG6043 airfoil has the best performance for almost all the working range of angles of attack; therefore, it is selected for building the studied model. The selected airfoil may not have the lowest C_d , yet has high enough C_l to compensate for this disadvantage and give the highest C_l/C_d ratio. A greater lift-to-drag ratio is considered one of the most aims in the design. The aerodynamic shape of the SG6043 airfoil is shown in Figure 4, which exhibits a gradual stall.

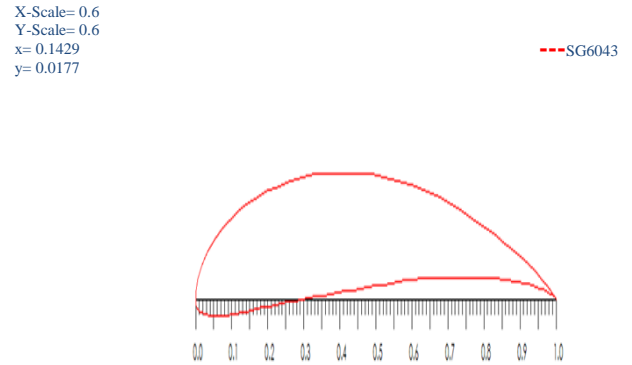


Figure 4. Cross section of airfoils SG6043 with span ratio.

For all the selected airfoils of small horizontal wind turbine blades, as the angle of attack increases, the lift coefficient increases till certain angle changes; according to the airfoil shape, the lift coefficient starts to decrease due to flow separation at this angle. The airfoil SG6043 has the highest lift coefficient and the flow separation occurs at the angle of attack 15° .

At low wind speeds, the power must be obtained at a high angle of attack. At these high angles, it is challenging to produce sufficient lift to turn the blades and the turbine operates at low performance due to laminar separation [25].

The airfoil SG6043 has the least drag coefficient for the working range of the angles of attack. Lift coefficient and drag coefficient curves are very close in the first range of the angles of attack; however, they have become obviously different in the range where the attack angle is behind the stall angle. Figure 2 shows that, after the stall angle, the drag coefficient sharply increases. The angle of attack at the stall point has different values due to different shapes of the airfoils.

The observed laminar separation results in low efficiency due to an increase in the drag, a decrease in the lift, and a change in the effective airfoil shape. This separation must be recognized and diminished in the airfoil design, especially at low wind speeds [26].

SG6043 airfoil data are inserted into QBlade to obtain its pressure distribution and boundary layers conditions.

For the selected airfoil SG6043, Figure 5 shows the variation of the ratio of lift coefficient to drag coefficient with the angle of attack. The maximum ratio satisfied at 4° angle of attack indicates that the lift is highly attained compared to drag, which is desirable in the design of a small wind turbine. The rotor torque and power generation are affected by the lift-to-drag ratio, especially at low wind speed.

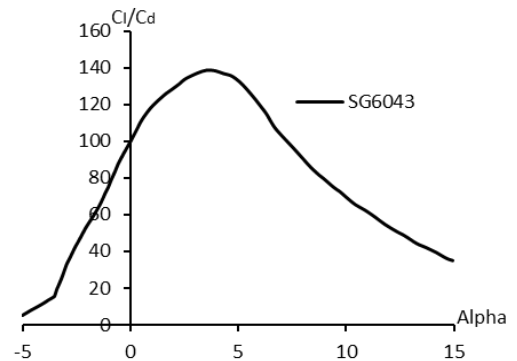


Figure 5. Ratio of lift coefficient to drag coefficient vs angle of attack relation at $Re=5*10^5$.

The aerodynamic performance of the Airfoil SG6043 is shown clearly in Figure 6, [26]. Figure 6 shows the drag polar (C_l vs C_d) and the relations among C_l , C_d , C_m , and C_l/C_d with the angle of attack in the range of -5 to 15 degree at different Reynolds numbers. All behaviors of SG6043 at different Reynolds numbers are in agreement; hence, at low wind speeds, the small variation of Reynolds number has no significant effect on the aerodynamic behaviors.

Figures 7a and 8a show the upper and lower surface pressure distribution of the airfoil and the resultant pressure force is changed according to the angle of attack. The lift force is produced at the leading area of the airfoil, because the pressure difference is greater than the trailing area.

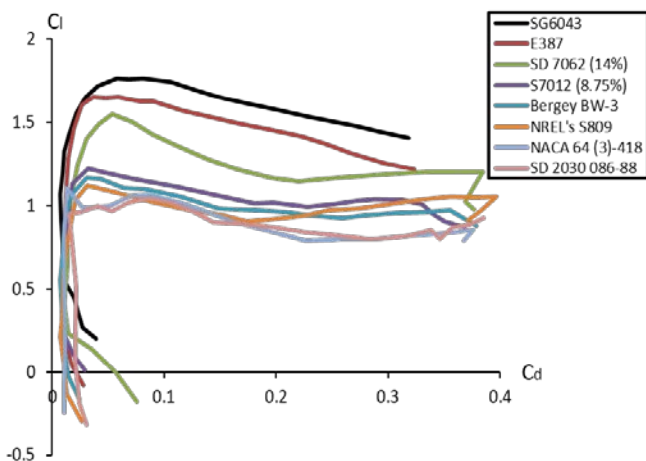


Figure 3. Lift coefficient-drag coefficient relations for different airfoils at $Re=5*10^5$.

Figures 7b and 8b show that, at low Reynolds number, the flow is separated at the leading area of the airfoil and alters from the lower surface to the upper surface of the airfoil as the angle of attack changes. The separated flow is recombined distant away from the trailing edge of the airfoil. This flow separation decreases the aerodynamic performance and the extracted power from the wind turbine [27].

4. METHODOLOGY AND BLADE DESIGN ALGORITHM

This research presents the design of the rotor blade performance for a small horizontal wind turbine at low operating wind speed based on blade element momentum theory (BEM). In this study, airfoil SG 6043 was selected by means of XFOIL software, considering the lift and drag

coefficients as reference parameters on the selected airfoils. The study was conducted for a variable chord with blade number 3 and a rotor radius of 1.25 m. The pitch angle varied from -5° to 25° . These values of blades' geometrical parameters generated in MATLAB are exported to Qblade software, producing results in terms of power coefficient, thrust coefficient, and torque coefficient curves with a tip speed ratio. The obtained results from Qblade must be verified numerically through computational fluid dynamic software and experimentally. The final design parameters modeled in SOLIDWORK are obtained by means of MATLAB. Figure 9 is a flowchart that shows the sequence of blade design methodology and the used algorithm.

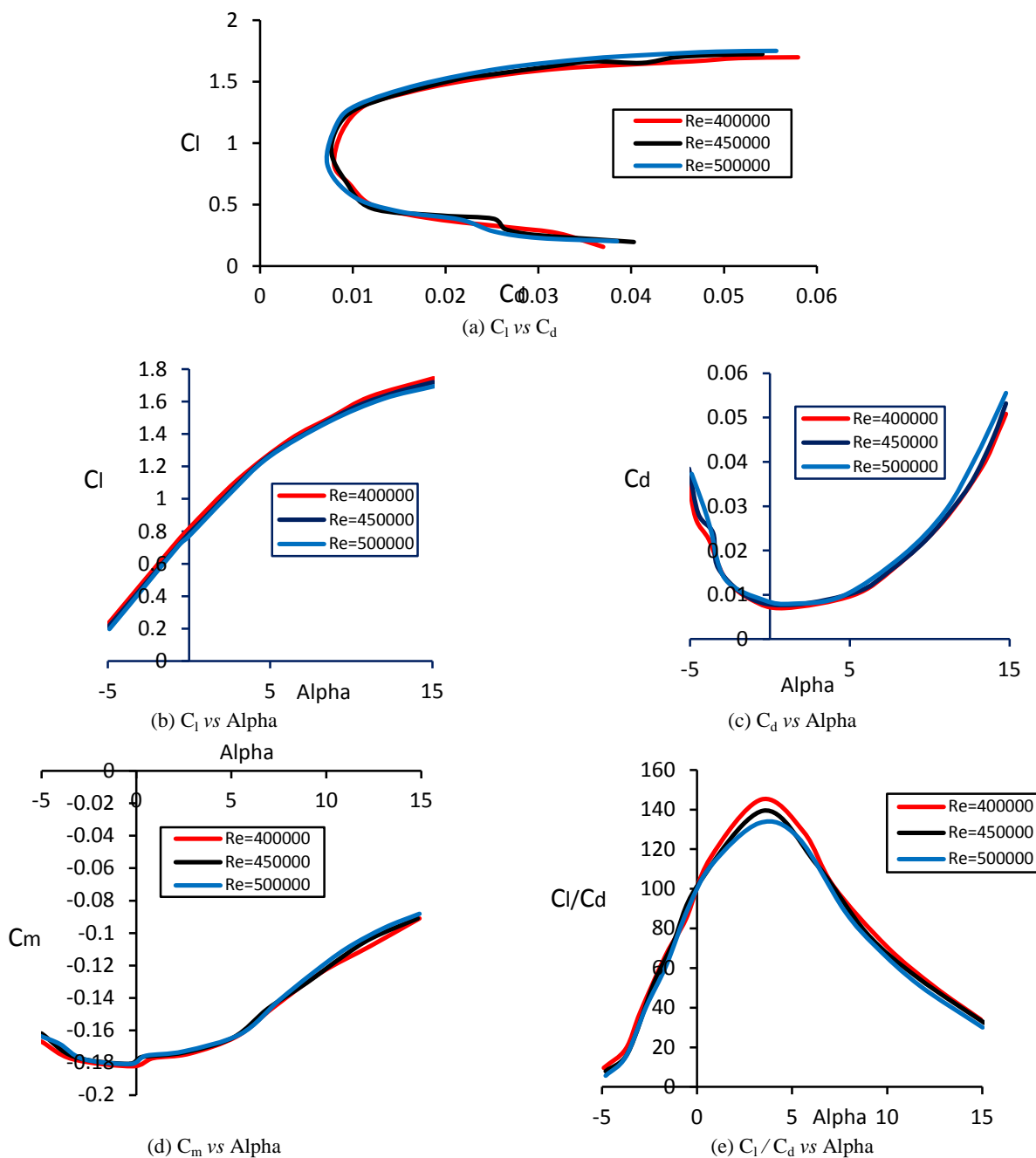
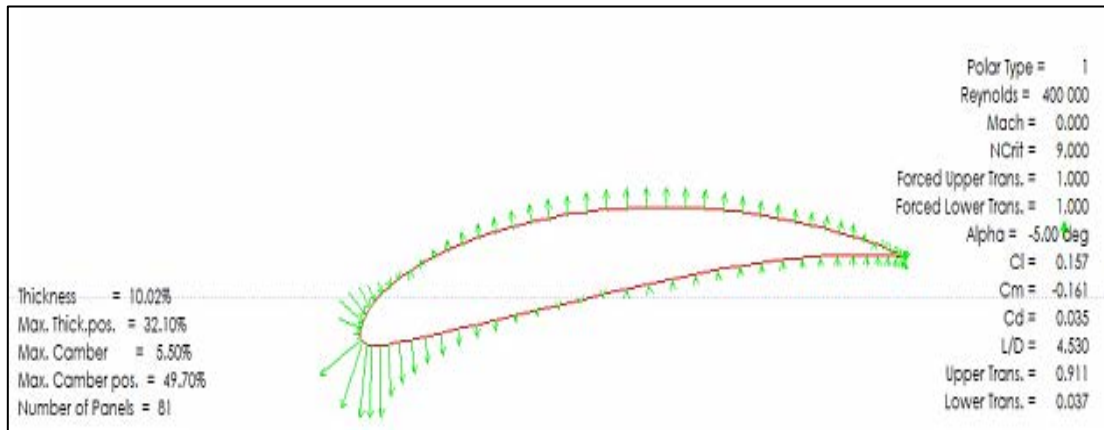
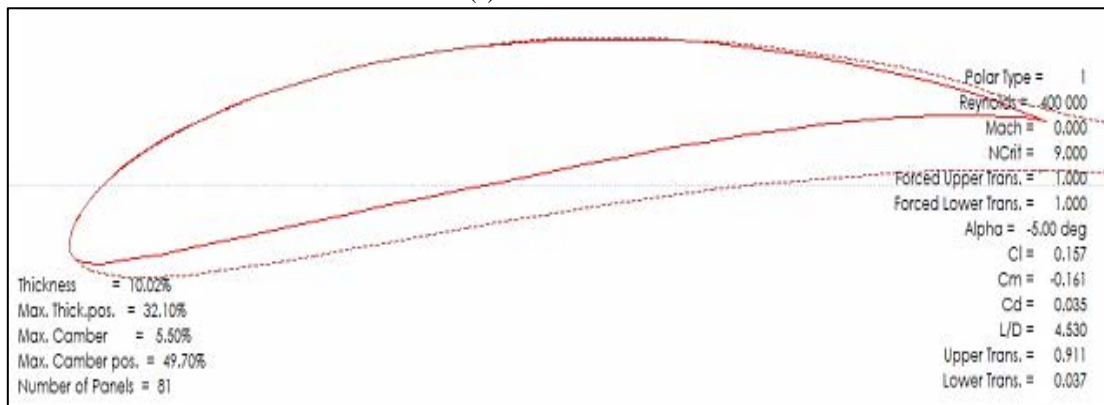


Figure 6. Airfoil SG6043 characteristics with $Re= 4 \cdot 10^5$, $Re= 4.5 \cdot 10^5$ and $Re= 5 \cdot 10^5$.

SG6043
 T1_Re0.400_M0.00_NP.0
 T1_Re0.450_M0.00_NP.0
 T1_Re0.500_M0.00_NP.0

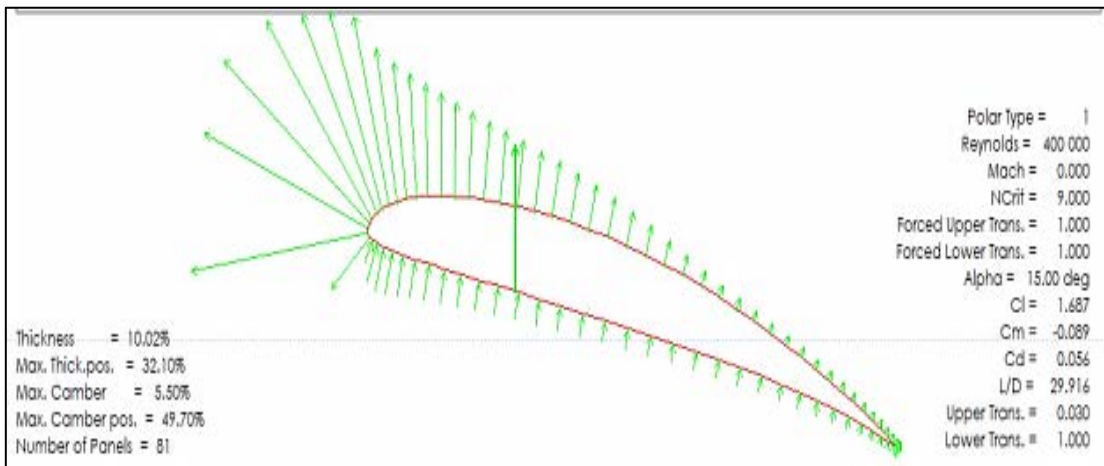


(a) Pressure vector

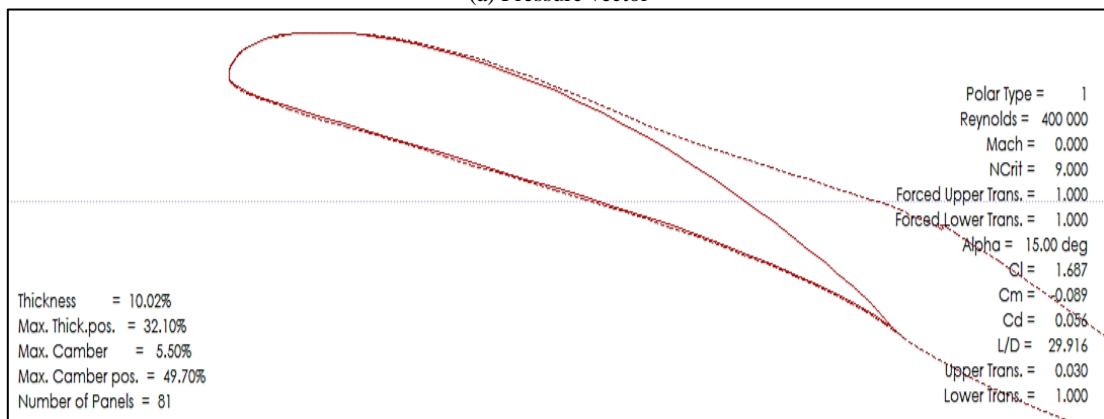


(b) Boundary layers

Figure 7. Flow visualization around airfoil at $\alpha=-5^\circ$ and $Re=4*10^5$.



(a) Pressure vector



(b) Boundary layers

Figure 8. Flow visualization around airfoil at $\alpha=15^\circ$ and $Re=4*10^5$.

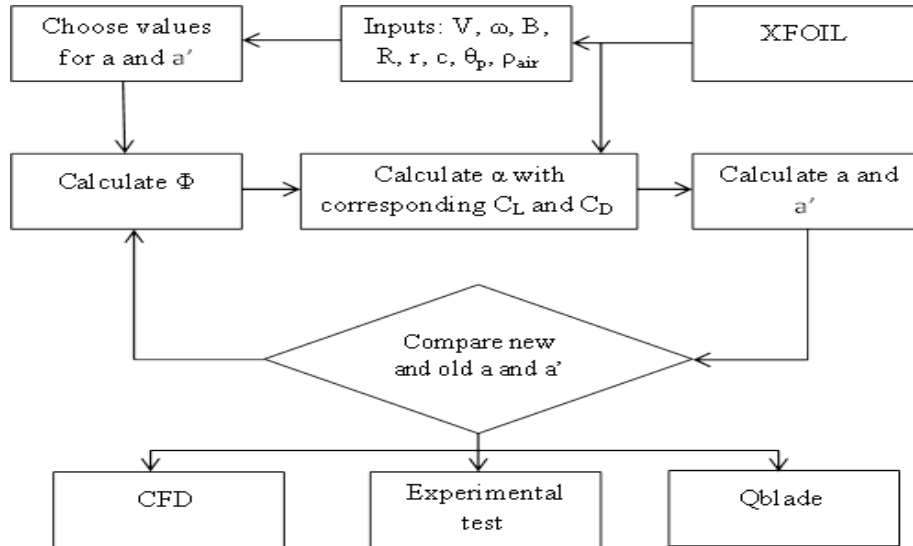


Figure 9. Flow diagram of the Iteration process and methodology for blade design algorithm.

5. MATHEMATICAL MODELING OF BLADE DESIGN

Blade Element Momentum (BEM) theory is a combination of blade element theory and momentum theory, corresponding to rotor geometry and rotor performance [10].

Blade element theory determines the performance of the blade by integrating the flow at each divided element of the blade along the span [28].

$$C_p = \frac{P}{\frac{1}{2}\rho AU^3} = 4a(1-a)^2 \quad (1)$$

where C_p is the power coefficient, P is power, ρ is the air density, A is the swept area of rotor, U is the wind velocity, and a is the axial induction factor. $C_{p,max}=0.5926$ at $a = 1/3$, [29].

The local tip speed ratio, λ_r , for each blade element is calculated by:

$$\lambda_r = \frac{\Omega r}{U} = \frac{\lambda_r}{R} = \left[\frac{a(1-a)}{a'(1-a')} \right]^{\frac{1}{2}} \quad (2)$$

where Ω is the rotor angular velocity, a' is the tangential induction factor, r is the radius of blade element, and R is the blade tip radius.

$$\Phi = \alpha + \theta_p \quad (3)$$

$$\theta_p = \theta_T + \theta_{p,o} \quad (4)$$

where θ_p is the pitch angle of section, $\theta_{p,o}$ is the pitch angle of the blade, θ_T is the twist angle of section, α is the angle of attack, and Φ is the relative wind angle.

$$c(r) = \frac{4\pi r F \sin \Phi}{BC_L \left\{ \left[\frac{\lambda_r + \tan \Phi}{1 - \lambda_r \tan \Phi} \right] - \left(\frac{C_D}{C_L} \right) \right\}} \quad (5)$$

where $c(r)$ is the blade chord length, $\frac{C_D}{C_L}$ is the minimum drag-to-lift ratio, F is the tip loss factor, C_L is the lift coefficient, and σ is the local solidity.

$$C_L = \frac{4F \sin \Phi (\cos \Phi - \lambda_r \sin \Phi)}{\sigma (\sin \Phi + \lambda_r \cos \Phi)} \quad (6)$$

$$C_L = \frac{4F \sin \Phi (\cos \Phi - \lambda_r \sin \Phi)}{\sigma (\sin \Phi + \lambda_r \cos \Phi)} \quad (7)$$

$$\sigma = \frac{BC(r)}{2\pi r} \quad (7)$$

In MATLAB, the tip loss correction factor is assumed to be 1 for simplicity and any divergence in the calculations is avoided ($0 < F_{tip} < 1$, along 80 % of blade length, its value equals unity).

$$F_{tip} = \frac{2}{\pi} \cos^{-1} \left\{ \exp \left[-\frac{B \left(1 - \frac{r}{R} \right)}{2 \left(\frac{r}{R} \right) \sin \Phi} \right] \right\} \quad (8)$$

$$F_{tip} = \frac{2}{\pi} \cos^{-1} \left\{ \exp \left[-\frac{B \left(1 - \frac{r}{R} \right)}{2 \left(\frac{r}{R} \right) \sin \Phi} \right] \right\} \quad (9)$$

$$a = \frac{1}{\frac{4F \sin^2 \Phi}{\sigma C_L \cos \Phi} + 1} \quad (9)$$

$$a' = \frac{1}{\frac{4F \cos \Phi}{\sigma C_L - 1} + 1} \quad (10)$$

Table 1. Blade design specifications.

Span (m)	Chord (m)	Flow Angle (φ)	Axial Induction Factor (a)	Tangential Induction Factor (a')
0.25	0.2	27.87	0.3532	0.18
0.3	0.19	25.9	0.3274	0.1298
0.4	0.18	20.2265	0.3575	0.0817
0.5	0.16	16.8611	0.3588	0.0542
0.6	0.14	14.7642	0.3426	0.0376
0.7	0.125	13.0272	0.3337	0.0275
0.8	0.11	11.929	0.3097	0.0204
0.9	0.1	10.8262	0.3003	0.0159
1	0.09	10.0499	0.2821	0.0125
1.1	0.085	8.6687	0.3216	0.0111
1.2	0.08	7.784	0.3375	0.0096
1.25	0.08	7.6428	0.3232	0.0087

This design is accomplished by MATLAB code to obtain accurate results with an error less than 10^{-5} . In the design, the number of blades $B=3$, the tip speed ratio $\lambda=5$, rotor radius $R=1.25m$, and the number of blade segments $N=10$. The blade geometry (optimal blade chord distributions along the span) is depicted in Table 1 and Figure 10. In some cases, the blade needs some modifications due to the manufacturing limits.

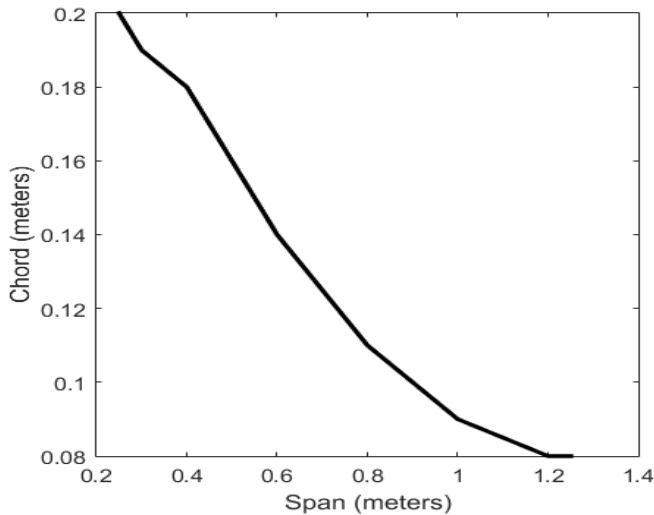


Figure 10. Chord distribution along the blade span for SG6043 airfoil.

6. BLADE PERFORMANCE

As shown in Figure 11, the thrust coefficient is 0.9 when the tip speed ratio equals 5; if this ratio decreases, the thrust coefficient sharply decreases. The moment coefficient has the maximum value at a tip speed ratio of 5; afterwards, it decreases, as shown in Figure 12.

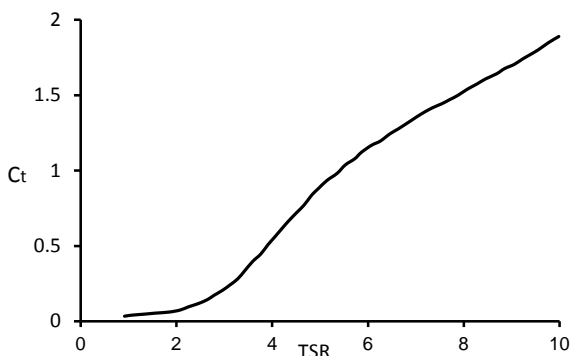


Figure 11. Thrust coefficient vs tip speed ratio relation for SG6043 airfoil.

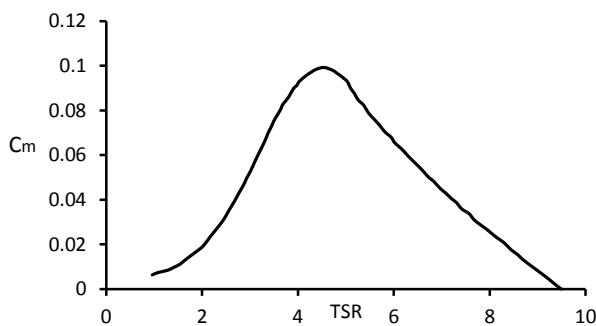


Figure 12. Torque coefficient vs tip speed ratio relation for SG6043 airfoil.

Figure 13 shows the maximum power coefficient with a value of 0.46 at the designed tip speed ratio that equals 5. Compared with other research studies, the maximum power coefficient obtained using the proposed design increases from 0.37 to 0.46 for the same airfoil and tip speed ratio [30]. In addition, the obtained maximum power coefficient has nearly the same value in approximately the same working conditions for other research studies [10].

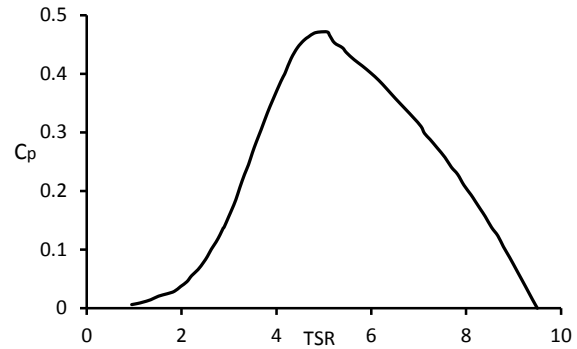


Figure 13. Power coefficient vs tip speed ratio relation for SG6043 airfoil.

Based on the linear relation between the rotation speed of the rotor and the tip speed ratio, shown in Figure 14, the tip speed ratio value of 5 corresponds to a rotation speed rate of 267.5 rpm, where maximum power is achieved.

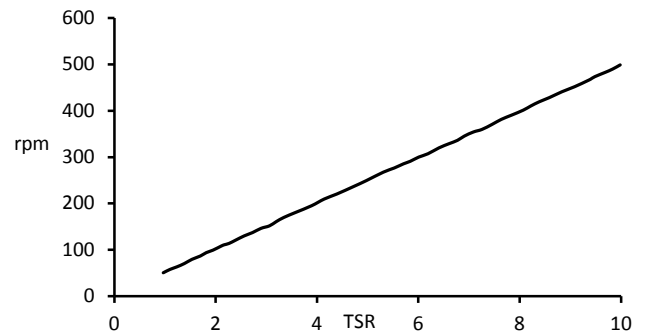


Figure 14. Rotor rotation speed vs tip speed ratio relation for SG6043 airfoil.

7. COMPUTATIONAL FLUID DYNAMICS (CFD)

The blades were modeled using SOLDWORK according to the provided data from MATLAB, as shown in Figure 15.



Figure 15. The blades CAD Design.

The simulations used in this research were performed by ANSYS Fluent software. The theoretical models used for these simulations include the Reynolds-Averaged Navier-Stokes (RANS) equations in combination with Shear-Stress Transport (SST) $k-\omega$ model [8]. The present horizontal axis wind turbine design consists of three frames with angles 120° between each one [11]. To simulate this process, the fluid domain geometry must be created by a cylinder with a dimension of 10m diameter and height of 5m, as shown in Figure 16.

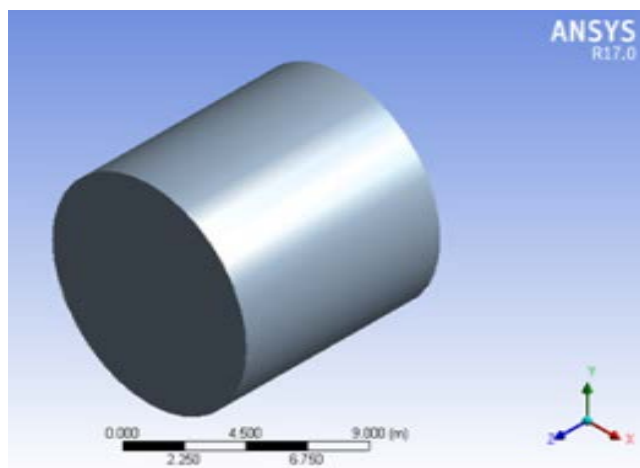


Figure 16. Schematic of the whole domain.

7.1. Meshing the domain

Global mesh controls were applied to the whole mesh altogether. Local mesh control was implemented to the areas right behind the turbine using mesh setting to capture all physical effects in these highly turbulent areas, [12]. Inflation is used to generate thin cells adjacent to boundaries and the wall $y+$ is satisfactorily obtained, thus helping resolve viscous boundary layer in CFD and high-stress concentration regions, as shown in Figure 17.

To check the mesh stability, calculations were repeated for a wide range of mesh sizes (from 1,000,000 to 3,000,000 cells). The decision when values of the drag and lift coefficients reach the steady state which satisfied after the mesh size of 2,500,000 cells. Thus, the grid consisted of 1880073 tetrahedral and 246140 wedge cells with 454031 nodes. In the distant region, the mesh becomes coarser due to the gradients of the flow, which can be neglected as shown in Figure 18.

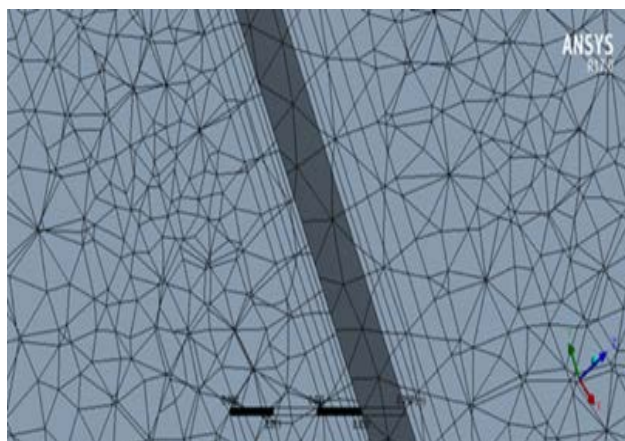


Figure 17. Effect of Inflation on the blade boundaries.

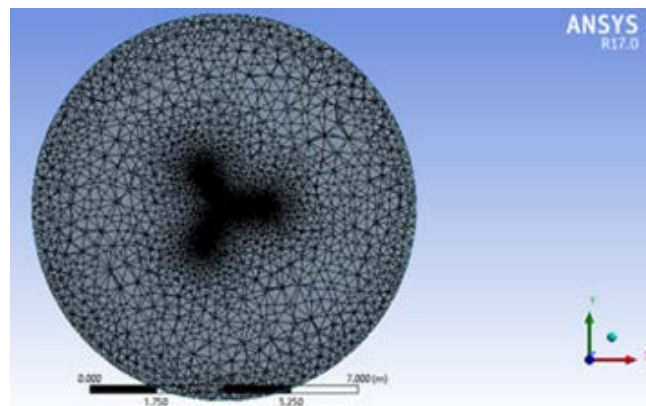
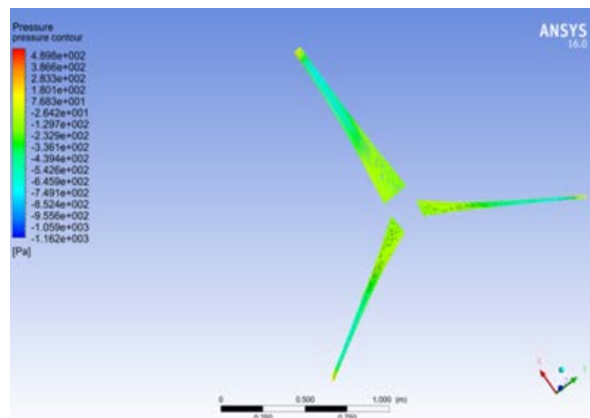


Figure 18. Effect of Body of influence relative to the whole mesh.

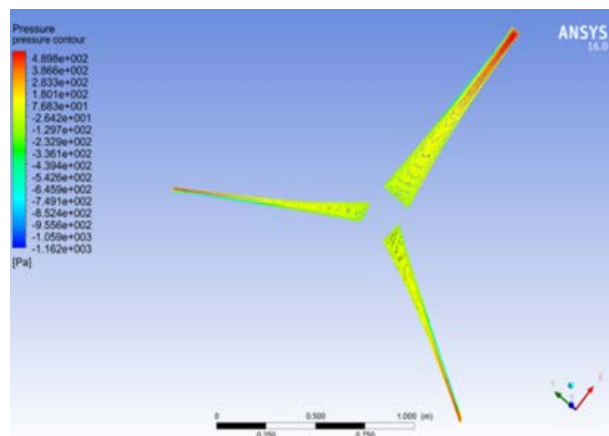
7.2. CFD results and discussion

Computational Fluid Dynamics analysis of the blade model was done in ANSYS Fluent 16. The used solver was pressure-based with a $k-\omega$ SST viscous model. In addition, the frame motion was enabled in z-direction with an angular velocity of -28rad/sec . The boundary conditions include velocity input and pressure outlet with a coupled solution method and 1500 iterations. The pressure and velocity contours on the blade surfaces were observed and analyzed.

Figures 19.a and 19.b show pressure contours on the upper and lower surfaces of the blade. Pressure on the lower side is relatively higher than that on the upper side, especially in the tip zone of the blade. This creates a net upward force that produces a lift.



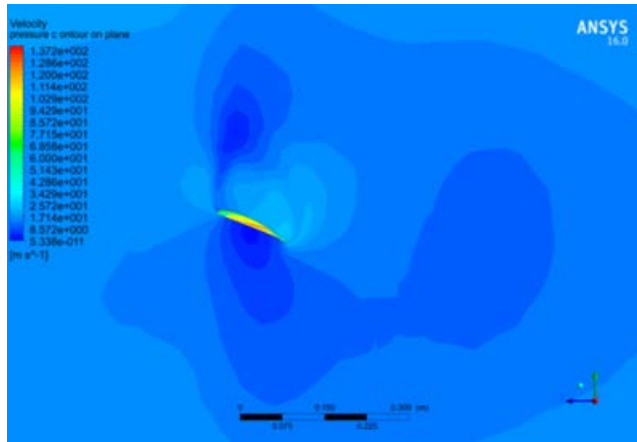
(a) Upper skin



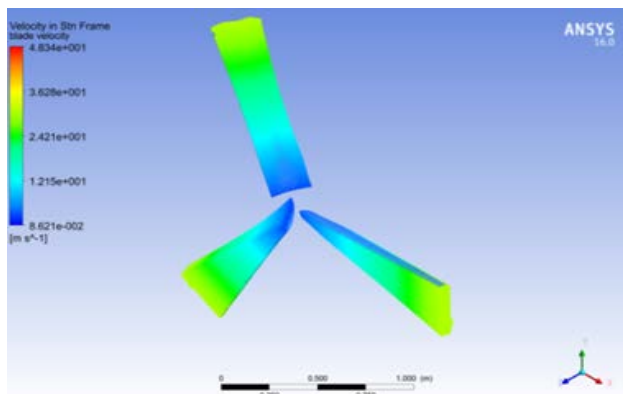
(b) Lower skin

Figure 19. Pressure contours of the blades.

The velocity field around the upper and lower surfaces of the blade is illustrated in Figures 20.a and 20.b. Observations reveal that the velocity values on the lower surface are lower than those on the upper surface. Figure 21 shows the streamlines around the blades that clearly show the wake rotation.



(a) Upper skin



(b) Lower skin

Figure 20. Velocity field of the blades.

Due to the wind stresses, it is obvious that the maximum shear stresses occur at the blade tip, as shown in Figure 22. Therefore, the leading edge must receive great care in manufacturing to avoid any prone to malfunctioning during the operation. The power obtained from CFD simulation was 268.52 watt.

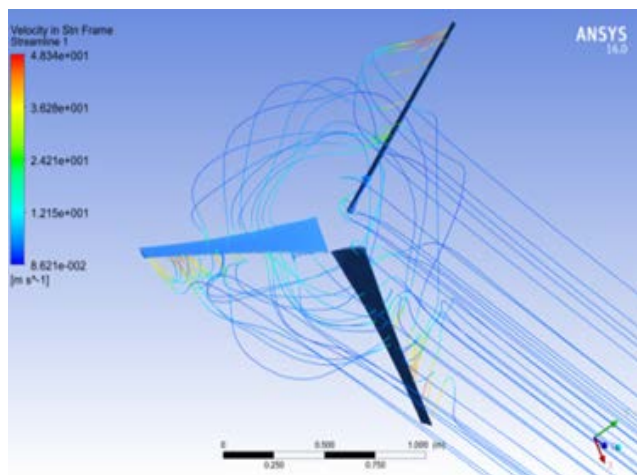


Figure 21. Streamlines around the blades.

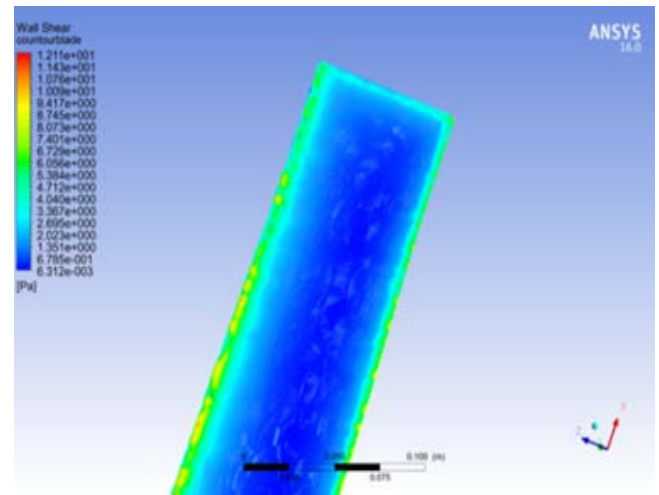


Figure 22. Shear stress at the blade tip.

8. FABRICATION OF THE BLADE

It is important to note that the manufacturing technique highly influences the quality of the finished parts and the extracted power. Hotwire cutter can be used as a new approach to blade manufacturing. Polyurethane foam is used to fabricate the blade due to its light weight, resiliency, low odor and high resistance, excellent cushioning, low cost, and easily cut to fit the blade design [31].

2D airfoil sections were imported from SOLIDWORK and, then, were cut by a laser cutting machine using MKF wood material, as shown in Figure 23. They are used as a guide; therefore, the hot wire can move around them to construct the required blade with correct shape and angles.



Figure 23. 2D airfoil sections.

The hot wire cutter is a device consisting of a thin, firm metal wire of stainless steel heated through electrical resistance to about 200 °C. Since the wire has passed through the foam material, the heat from the wire vaporizes the foam just in contact.

Surface finishing by the sandpaper was done to ensure that the dimensions of blade segments and leading edge is crafted perfectly. A hole was conducted along all the segments (4 segments for each blade) to give a space for the iron rod to connect the segments together and give them more strength and, finally, to support the blade with hub, as shown in Figure 24.



Figure 24. Photo of assembled blade.

Finally, a layer of paste was added to increase the strength of the blade, fill out any holes in the foam, reduce any dynamic instability, provide a smooth surface, and obtain the final dimensions of the blade [32]. A circular metal disc is used as a rotor hub. It is crucial for the blades to be attached symmetrically; otherwise, imbalances may cause oscillations, which can lead to a blade tearing away from the hub, as shown in Figure 25.a, which imitates the CAD design in Figure 25.b. A permanent magnet DC motor driven in reverse was used as a generator.



(a) Photo



(b) CAD

Figure 25. Small horizontal wind turbine.

9. EXPERIMENTAL RESULTS AND DISCUSSION

Related tests have been conducted on the roof of Ismailia engineering college campus. With an average wind speed of 4 m/s, measurements were taken by connecting the output of the generator with a multi-meter to measure the voltage. The wind speed was measured by a cup anemometer. The electrical

power measured at this average speed is 9 watt. This low value of the output power generated from the wind turbine results from low average wind speed and the inaccuracy with some deviations in the blade configuration during the fabrication and measuring processes, resulting in low turbine efficiency. In addition, the flow separation due to laminar flow is considered a reasonable source for low power output. This low energy has been applicable to lightening houses, battery charging, and remote areas. Therefore, the choice of the wind turbine site is essential, since the maximum power that can be theoretically extracted from the designed wind turbine is 110 watts. The efficiency of the fabricated small horizontal wind turbine is 8 %. The generated power is considered to be accepted as compared with other researches [33 & 10].

10. CONCLUSIONS

This study investigated the performance of small wind turbine blades in low wind speed areas. The investigation used the BEM and CFD approaches. The application of XFOIL software facilitated airfoils selection at low different Re numbers. SG6043 airfoil was selected. Exporting the data to Q-blade program allows for the visualization and analysis of airfoil performance. Maximum power coefficient is 0.46 as obtained at a tip speed ratio equal to 5, corresponding to the rotor's rotation speed of 267.5 rpm. Such CFD results as pressure contour, velocity field, stream lines, and shear stress on the blades are appreciated. The blades are successively fabricated and assembled according to the design and succeeded to supply electricity with an average power 9watt and efficiency 8 %.

11. ACKNOWLEDGEMENT

The authors acknowledge the wind turbine team (MUDIM) for the submitted effort and the financial support of National Telecommunications Regulatory Authority (NTRA) of Egypt.

REFERENCES

1. Tong, W., Fundamentals of wind energy, Kollmorgen Corporation, Virginia, USA, (2010). (http://www.akenergyauthority.org/Content/Programs/AEEE/Reports_and_Presentations/Fundamentals-of-Wind_Ian-Baring-Gould_NREL.pdf).
2. Burton, T., Jenkins, N., Sharpe, D. and Bossanyi, E., Wind energy handbook, 2nd ed. John Wiley and Sons Ltd., Chichester, (2011). (https://www.researchgate.net/wind_turbine/attachment/AS3A273535103111175).
3. Ministry of Electricity & Renewable Energy, New & Renewable Energy Authority (NREA), Egypt's renewable energy activities and strategy, (2017). (<https://sustainabledevelopment.un.org/content/documents/22372Dr.MohamedElSobki.pdf>).
4. Clean energy development in Egypt, African Development Bank, (2012). (https://www.afdb.org/fileadmin/uploads/afdb/Documents/Policy-Documents/Cata_Energie_Anglais.pdf).
5. Renewable energy in Egypt, the green opportunity, (February 2017). (<https://www.slideshare.net/RoshdyAbdelrassoul1/renewable-energyinyegyptthegreenopportunity>).
6. Wang, Z., Tian, W. and Hu, H., "A comparative study on the aeromechanic performances of upwind and downwind horizontal-axis wind turbines", *Energy Conversion and Management*, Vol. 163, (2018), 100-110. (DOI: 10.1016/j.enconman.2018.02.038).
7. Selig, M., Gopalarathnam, A., Giguere, P. and Lyon, C., "Systematic airfoil design studies at low Reynolds numbers", *Proceedings of The Conference on Fixed, Flapping and Rotary Wing Vehicles at Very Low Reynolds Numbers*, Notre Dame, (2000), 5-7. (<https://doi.org/10.2514/5.9781600866654.0143.0167>).
8. Costa Rocha, P.A., Barbosa Rocha, H.H., Moura Carneiro, F.O., Vieira da Silva, M.E. and Freitas de Andrade, C., "A case study on the

- calibration of the $k-\omega$ SST (shear stress transport) turbulence model for small scale wind turbines designed with cambered and symmetrical airfoils", *Energy*, Vol. 97, (2016), 144-150. (<https://doi.org/10.1016/j.energy.2015.12.081>).
9. Bai, C.J., Hsiao, F.B., Li, M.H., Huang, G.Y. and Chen, Y.J., "Design of 10 kW horizontal-axis wind turbine (HAWT) blade and aerodynamic investigation using numerical simulation", *Proceedings of 7th Asian-Pacific Conference on Aerospace Technology and Science, Procedia Engineering*, Vol. 67, (2013), 279-287. (<https://doi.org/10.1016/j.proeng.2013.12.027>).
 10. Kumar Chaudhary, M. and Roy, A., "Design & optimization of a small wind turbine blade for operation at low wind speed", *World Journal of Engineering*, Vol.12, (2015), 83-94. (DOI: 10.1260/1708-5284.12.1.83).
 11. Abrar, M.A., Mahhub, A.M.I. and Mamun, M., "Design optimization of a horizontal axis micro wind turbine through development of CFD model and experimentation", *Procedia Engineering*, Vol. 90, (2014), 333-338. (<https://doi.org/10.1016/j.proeng.2014.11.858>).
 12. Jebarose Juliyana, S., Udaya Prakash, J., Karthik, K., Pallavi, P. and Saleem M., "Design and analysis of NACA4420 wind turbine aero-foil using CFD", *International Journal of Mechanical Engineering and Technology*, Vol. 8, No. 6, (2017), 403-410. (https://www.iaeme.com/MasterAdmin/uploadfolder/IJMET_08_06_042/IJMET_08_06_042.pdf).
 13. Lee, M.-H., Shiah, Y.C. and Bai, C.-J., "Experiments and numerical simulations of the rotor-blade performance for a small-scale horizontal axis wind turbine", *Journal of Wind Engineering and Industrial Aerodynamics*, Vol. 149, (2016), 17-29. (<https://doi.org/10.1016/j.jweia.2015.12.002>).
 14. Durga Prasad, B. and Vishnu Vardhan, T., "Finite element analysis and experimental investigations on small size wind turbine blades", *International Journal of Mechanical Engineering and Technology*, Vol. 3, No. 3, (2012), 493-503. (<https://www.slideshare.net/iaemedu/finite-element-analysis-and-experimental-investigations-on-small-size-wind-turbine-blades>).
 15. Koc, E., Günel, O. and Yavuz, T., "Comparison of Q-blade and CFD results of small scaled horizontal axis wind turbine analysis", *5th International Conference on Renewable Energy Research and Applications*, UK, (2016). (DOI: 10.1109/ICRERA.2016.7884538).
 16. Ali, A., Chowdhury, H., Loganathan, B. and Alam, F., "An aerodynamic study of a domestic scale horizontal axis wind turbine with varied tip configurations", *Procedia Engineering*, Vol. 105, (2015), 757-762. (<https://doi.org/10.1016/j.proeng.2015.05.067>).
 17. Pambudi, N.A., Pristiandaru, D.L., Basori, Wijayanto, D.S., Sriwardani, N., Rahman, N., Bugis, H., Wahyudi, B.D., Sudibyo, C., Karno, M.W. and Subagsono, "Experimental investigation of wind turbine using nozzle-lens at low wind speed condition", *Energy Procedia*, Vol. 105, (2017), 1063-1069. (<https://doi.org/10.1016/j.egypro.2017.03.459>).
 18. Dilimulati, A., Stathopoulos, T. and Paraschivoiu, M., "Wind turbine designs for urban applications: A case study of shrouded diffuser casing for turbines", *Journal of Wind Engineering and Industrial Aerodynamics*, Vol. 175, (2018), 179-192. (<https://doi.org/10.1016/j.jweia.2018.01.003>).
 19. Mohammadi, M.R., Mohammadi, A.R., Mohammadi M. and Neisi Minaei, H., "Optimization of small scale wind turbine blades for low speed conditions", *International Journal of Clean Energy Technologies*, Vol.4, No. 2, (2016), 140-143. (DOI: 10.7763/IOCET.2016.V4.268).
 20. Oluseyi, A., Opeyemi, O., Abiodun, A.S., Akinwale, A. and Alex, W., "Novel airfoil design for small horizontal axis wind turbine: A preliminary result", *Proceedings of Third Southern African Solar Energy Conference*, (2015), 181-186. (http://eprints.covenantuniversity.edu.ng/7388/1/Ajayi_Novel_2015%281%29.pdf).
 21. Wright, A.K. and Wood, D.H., "The starting and low wind speed behavior of a small horizontal axis wind turbine", *Journal of Wind Engineering and Industrial Aerodynamics*, Vol. 92, (2004), 1265-1279. (<https://doi.org/10.1016/j.jweia.2004.08.003>).
 22. Singh, R.K., Rafiuddin Ahmed, M., Zullah, M.A. and Lee, Y.-H., "Design of a low Reynolds number airfoil for small horizontal axis wind turbines", *Renewable Energy*, Vol. 42, (2012), 66-76. (<https://doi.org/10.1016/j.renene.2011.09.014>).
 23. Somers, D.M. and Tangler, J.L., "NREL airfoil families for HAWTs", *National Renewable Energy Laboratory*, (1995). (DOI: 10.2172/10106095).
 24. Drela, M., "XFOIL subsonic airfoil development", (<http://web.mit.edu/drela/public/web/xfoil/>, 1986).
 25. Selig, M.S. and McGranahab, B.D., "Wind tunnel aerodynamic tests of six airfoils for use on small turbines", *National Renewable Energy Laboratory*, (2004). (DOI: 10.1115/1.1793208).
 26. Kale, S.A. and Varma, R.N., "Aerodynamic design of a horizontal axis micro wind turbine blade using NACA 4412 profile", *International Journal of Renewable Energy Research*, Vol. 4, No. 1, (2014). (<https://www.researchgate.net/publication/261170924>).
 27. Karthikeyan, N., Kalidasa Murugavel, K., Arun Kumar, S. and Rajakumar, S., "Review of aerodynamic developments on small horizontal axis wind turbine blade", *Renewable and Sustainable Energy Reviews*, Vol. 42, (2015), 801-822. (<https://doi.org/10.1016/j.rser.2014.10.086>).
 28. Navin Prasad, E., Janakiram, S., Prabu, T. and Sivasubramaniam, S., "Design and development of horizontal small wind turbine blade for low wind speeds", *International Journal of Engineering Science & Advanced Technology*, Vol. 4, (2014), 75-84. (http://ijesat.org/Volumes/2014_Vol_04_Iss_01/IJESAT_2014_01_01_14.pdf).
 29. Kanyako, F. and Janajreh, I., "Investigating blade performance of small horizontal axis wind turbine based on blade element momentum theory", *1st International Conference & Exhibition on the Applications of Information Technology to Renewable Energy Processes and Systems*, Amman, Jordan, (2013). (DOI: 10.1109/IT-DREPS.2013.6588158).
 30. Khaled, M., Ibrahim, M.M., Abdel Hamed, H.E. and Abdel Gawad A.F., "Aerodynamic design and blade angle analysis of a small horizontal-axis wind turbine", *American Journal of Modern Energy*, Vol. 3, No. (2), (2017), 23-37. (doi: 10.11648/j.ajme.20170302.12).
 31. Aitchison, D., Brooks, H., Bain, J. and Pons, D., "An investigation into the prediction of optimal machining conditions for polystyrene foam cut with a taut hot-wire", *The Annals of "Dunarea de Jos" University of Galati Fascicle V*, (2009). (<http://www.if.ugal.ro/TMB/2009/I3.pdf>).
 32. Abeyasinghe, A., Abey Siriwar, S., Nanayakkarawasam, R., Wimal Siri, W., Lalitharatne, T. and Tennakoon, S., "Development of a numerically controlled hot wire foam cutting machine for wing mould construction", *Moratuwa Engineering Research Conference, Moratuwa*, Sri Lanka, (2016). (DOI: 10.1109/MERCon.2016.7480116).
 33. Sahin, A.Z., Al-Garni, A.Z. and Al-Farayedhi, A., "Analysis of a small horizontal axis wind turbine performance", *International Journal of Energy Research*, Vol. 25, (2001), 501-506. (DOI: 10.1002/er.699).